Investigations of Reactive Processes at Temperatures Relevant to the Hypersonic Flight Regime

Markus Meuwly

UNIVERSITAT BASEL
PETERSPLATZ 1
BASEL 4003 SWITZERLAND

Report Date: October 2014

Final Report from 1 December 2012 to 28 February 2014

REPORT DOCUMENTATION PAGE			Form Approved OMB No. 0704-0188

Public reporting burden for this collection of information is estimated to average 1 hour per response, including the time for reviewing instructions, searching existing data sources, gathering and maintaining the data needed, and completing and reviewing the collection of information. Send comments regarding this burden estimate or any other aspect of this collection of information, including suggestions for reducing the burden, to Department of Defense, Washington Headquarters Services, Directorate for Information Operations and Reports (0704-0188), 1215 Jefferson Davis Highway, Suite 1204, Arlington, VA 22202-4302. Respondents should be aware that notwithstanding any other provision of law, no person shall be subject to any penalty for failing to comply with a collection of information if it does not display a currently valid OMB control number. **PLEASE DO NOT RETURN YOUR FORM TO THE ABOVE ADDRESS.**

1. REPORT DATE *(DD-MM-YYYY)*	2. REPORT TYPE	3. DATES COVERED *(From – To)*
31 October 2014	Final Report	1 December 2012 – 28 February 2014

4. TITLE AND SUBTITLE	5a. CONTRACT NUMBER
Investigations of Reactive Processes at Temperatures Relevant to the Hypersonic Flight Regime	**FA8655-13-1-3014**
	5b. GRANT NUMBER
	Grant 13-3014
	5c. PROGRAM ELEMENT NUMBER
	61102F

6. AUTHOR(S)	5d. PROJECT NUMBER
Markus Meuwly	
	5d. TASK NUMBER
	5e. WORK UNIT NUMBER

7. PERFORMING ORGANIZATION NAME(S) AND ADDRESS(ES)	8. PERFORMING ORGANIZATION REPORT NUMBER
UNIVERSITAT BASEL PETERSPLATZ 1 BASEL 4003 SWITZERLAND	N/A

9. SPONSORING/MONITORING AGENCY NAME(S) AND ADDRESS(ES)	10. SPONSOR/MONITOR'S ACRONYM(S)
EOARD Unit 4515 APO AE 09421-4515	AFRL/AFOSR/IOE (EOARD)
	11. SPONSOR/MONITOR'S REPORT NUMBER(S)
	AFRL-AFOSR-UK-TR-2014-0041

12. DISTRIBUTION/AVAILABILITY STATEMENT

Distribution A: Approved for public release; distribution is unlimited.

13. SUPPLEMENTARY NOTES

14. ABSTRACT
Reactions involving nitrogen (N) and oxygen (O) atoms dominate the energetics of the reactive air flow around spacecraft when reentering the atmosphere in the hypersonic flight regime. One of the important determinants for the chemistry in such flows are the thermal rate coefficients for reactive processes. In the present project, rate coefficients are determined for reactions involving $O(^3P)$ and $NO(^2II)$. For this, a potential energy surface (PES) for the ground state of the NO_2 molecule is constructed based on high-level ab-initio calculations and interpolated using the reproducible kernel Hilbert space (RKHS) method and Legendre polynomials. The global PES of NO_2 in the ground state is constructed by smoothly connecting the surfaces of the grids of various channels around the equilibrium NO_2 geometry by a distance-based switching function. The rate coefficients are calculated from Monte Carlo sampling. The results indicate that at high temperatures primarily the lowest electronic state is relevant and zero-point effects are not relevant. The rate coefficient for O_2 production at 20,000 K becomes comparable (to within a factor of around three) to the rate coefficient of the oxygen exchange channel for the same temperature. The computational approach outlined and pursued is generic for small-molecule reactions and can be applied to other reactions relevant to the hypersonic flight regime.

15. SUBJECT TERMS

EOARD, hypersonic reactive processes, high-speed reaction chemistry

16. SECURITY CLASSIFICATION OF:			17. LIMITATION OF ABSTRACT	18, NUMBER OF PAGES	19a. NAME OF RESPONSIBLE PERSON
a. REPORT UNCLAS	b. ABSTRACT UNCLAS	c. THIS PAGE UNCLAS	SAR	15	Gregg L. Abate
					19b. TELEPHONE NUMBER *(Include area code)* +44 (0)1895 616021

Standard Form 298 (Rev. 8/98)
Prescribed by ANSI Std. Z39-18

<div align="center">

Report on:
Investigations of Reactive Processes at Temperatures
Relevant to the Hypersonic Flight Regime
Computational Chemistry Group, University of Basel

</div>

1 Overview

Reactions involving N and O atoms dominate the energetics of the reactive air flow around spacecraft when reentering the atmosphere in the hypersonic flight regime. One of the important determinants for the chemistry in such flows are the thermal rate coefficients for reactive processes. In the present project, rate coefficients are determined for reactions involving $O(^3P)$ and $NO(^2\Pi)$. For this, a potential energy surface (PES) for the ground state of the NO_2 molecule is constructed based on high-level *ab initio* calculations and interpolated using the reproducible kernel Hilbert space (RKHS) method and Legendre polynomials. The global PES of NO_2 in the ground state is constructed by smoothly connecting the surfaces of the grids of various channels around the equilibrium NO_2 geometry by a distance-based switching function. The rate coefficients are calculated from Monte Carlo sampling. The results indicate that at high temperatures primarily the lowest electronic state is relevant and zero-point effects are not relevant. The rate coefficient for O_2-production (the "O1O2+N" channel) at 20000 K becomes comparable (to within a factor of around three) to the rate coefficient of the oxygen exchange channel for the same temperature. The computational approach outlined and pursued is generic for small-molecule reactions and can be applied to other reactions relevant to the hypersonic flight regime.

2 Introduction

The computation of effective rate coefficients at arbitrary thermodynamic conditions is an essential aspect in modeling, understanding and characterizing the chemistry in the hypersonic flight regime. Direct experimentation at the relevant conditions (temperatures of up to 20000 K; nonequilibrium flow) is usually difficult or even impossible. Hence, an *in silico* approach holds much promise in providing the necessary input data for modeling the chemical networks.

Nitric dioxide (NO_2) is one of the molecules which plays an important role as a model system in atmospheric chemistry, as a smog constituent and in combustion processes.[1, 2, 3] While most of these processes occur close to thermal equilibrium and at moderate temperatures, reactions involving NO_2 have also attracted interest under more extreme conditions. This is the case for the hypersonic flight regime of spacecraft reentering the atmosphere. The chemistry at the surface of such vehicles typically involves highly non-equilibrium conditions with vibrational and rotational temperatures reaching several thousand Kelvin.[4] The gas-phase and surface reactions and energy transfer at these temperatures are essentially uncharacterized and the experimental methodologies capable of probing them are not well established. Under such circumstances, validated computational investigations become a valuable complementary tool.

In the present work, the formation of NO_2 from $NO(^2\Pi)$ and $O(^3P)$ and its subsequent dissociation into oxygen-exchange and O_2 formation channels is investigated. Characterizing the kinetics and dynamics of a chemical reaction from computation usually requires a potential energy surface for the interactions involved. Within the framework of Molecular Dynamics

(MD) simulations, this can either be an *ab initio*/semiempirical MD (AIMD) approach, a model potential energy surface (PES) or a parametrized, multidimensional PES fitted to electronic structure calculations, experimental observables, or a combination of the two.[5] Using AIMD is usually only possible for small systems and sufficiently short simulation times due to the considerable computational cost.[6, 7, 8] A more efficient approach is to use separate grids for the different regions of interest and join them smoothly. In the asymptotic regions, that is, reactants or products, the dynamics is carried out on a single and simpler PES leading to a faster simulation. In the intermediate regions, the global surface is represented as a weighted sum of the contributions of all individual PESs. This approach has been successfully applied to connect different force fields.[9] We will pursue a similar strategy in the present work to build a global PES for NO_2.

The aim of the present work is the characterization of the reaction between $O(^3P)$ and $NO(^2\Pi)$ at higher temperatures relevant to the hypersonic flight regime of reentering space-crafts. At a more fundamental level, we are particularly interested in establishing an efficient computational framework capable of probing small molecular systems for a wide range of parameters. The general approach is: (1) the construction of PESs for the ground state of the NO_2 molecule based on high-level *ab initio* calculations and their fitting with a reproducing kernel Hilbert space (RKHS) method combined with Legendre polynomials; (2) quasi-classical trajectory calculations to study the adiabatic reaction dynamics, and (3) calculation of the rate coefficients for the different exit channels using Monte Carlo method. The results of the simulations will be compared with previous computational[10, 11, 12] and experimental works[13] in order to validate the computational approach. In the context of the hypersonic flight regime, the O_2 production channel ($NO+O\rightarrow O_2+N$) is of particular interest since the thermal dissociation threshold for O_2 is lower than that for N_2 in air. A central question is how translational excitation of the reactants and vibrational excitations of the NO affect the rate coefficient of O_2 formation.

3 Methodology

3.1 *Ab initio* calculations

The present calculations use Dunning's standard correlation-consistent polarized quadruple (cc-pVQZ) basis set.[14, 15] For a meaningful description of the geometries and energetics of the NO_2 molecule, its dissociation energetics and the conical intersections between the ground and the low-lying excited states, a multiconfigurational method is required. For this, the complete active space self-consistent field (CASSCF) method is employed which takes into account static correlation. For recovering the dynamic correlation, e.g. during bond breaking and formation, multireference configuration interaction (MRCI) is used. The Davidson correction [16, 17] is included to estimate the effects of higher excitations (MRCI+Q). All calculations are performed with the MOLPRO program ver. 2012.1.[18]

Figure 1 gives a schematic representation of the general relevant stages of the reaction of interest. Initially, the $O(^3P)$ atom approaches the $NO(^2\Pi)$ molecule. Depending on the impact parameter b, the quantum state of the NO (vibrational and rotational) and the collision energy, the NO_2 molecule is formed. In the absence of additional collisional partners (zero pressure) the NO_2 will decay as it was formed with an energy above its dissociation limit. The following possibilities exist for the products: NO_2 can (1) dissociate into the same incoming
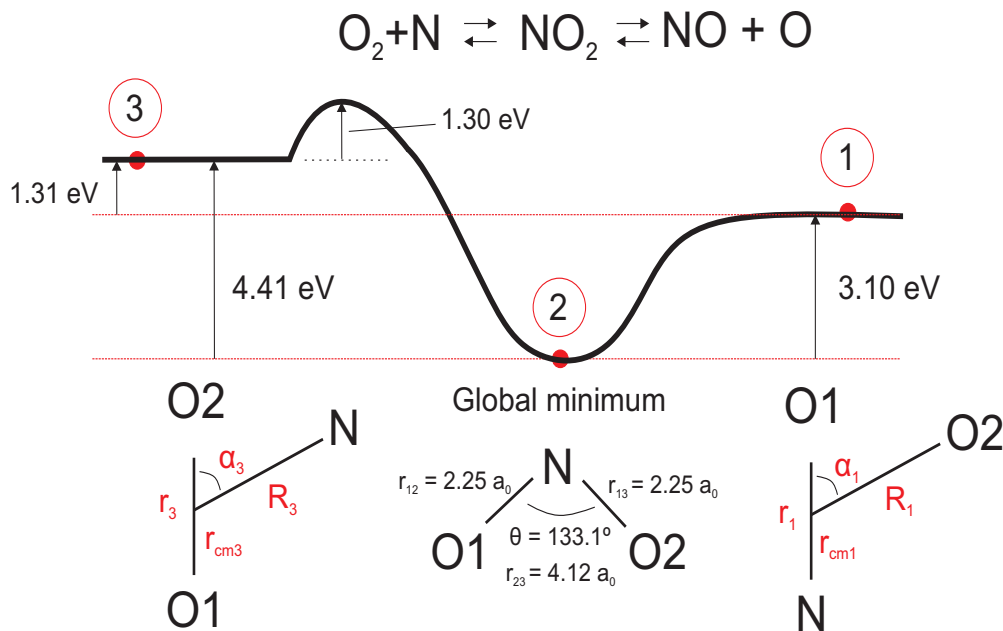
Figure 1: Relevant stages in the NO1+O2 reaction. The energies were derived from the *ab initio* calculations of this work.

constituents (NO1+O2→NO1+O2), (2) dissociate into the same constituents but with the oxygen atoms exchanged (NO1+O2→NO2+O1), (3) form dioxygen (O_2+N) or (4) atomize into the individual atoms (N+O1+O2). The latter is not further considered in this work.

In the presence of additional collisional partners, the NO_2 can loose its excess energy and can stabilize. In the high-pressure limit this takes place for all trajectories which enter the potential well of NO_2 and thereby it is straightforward to determine the high-pressure limit rate coefficient for NO_2 formation.

In order to describe the different channels, three grids in Jacobi coordinates are employed to systematically cover the relevant regions of the PES in the NO_2 system (Figure 1). The first grid (for the NO1+O2 asymptote) includes the coordinates r_1 (the N-O1 distance), R_1 (the distance from the center of mass of NO1 to the oxygen atom O2), and α_1 (the angle formed by O1, the center of mass of NO1 and O2 (Figure 1)). With this grid, the entrance (NO1+O2) and NO_2-formation channels can be described. For the oxygen exchange channel (NO2-O1), a permutation of the oxygens in the first grid is performed. As a result, the second grid is defined by r_2, R_2 and α_2. For the third grid (O1O2+N), r_3 is the O-O distance, R_3 is the distance from the center of mass of the O_2 molecule to the nitrogen atom and α_3, is the angle between O2, the center of mass of the O_2 molecule and the nitrogen atom (Figure 1).

For the r_1 and r_3 coordinates, 12 points ($n_r = 12$) from 1.7 to 2.55 a_0 were selected. As for the R_1 and R_3 coordinates, 29 points ($n_R = 29$) between 1.85 and 18.9 a_0 were selected. The α_1 and α_3 angles (in degrees) are from an 11-point ($n_\alpha = 11$) Gauss-Legendre quadrature ($\alpha = 11.98, 27.49, 43.10, 58.73, 74.36, 90.0, 105.64, 121.28, 136.9, 152.5, 168.02$). In total, 3828 points were calculated for each grid.

3.2 Representation of the PESs

In order to obtain the PESs of the NO_2 molecule from the *ab initio* energies, a reproducing kernel Hilbert space (RKHS) ansatz[19] for the distances (r and R) is combined with Legendre polynomials for the angles (α) (see Figure 1 for the Jacobi coordinates). First, for each combination (R,α) in the grid, a set of functions $V_{R,\alpha}(r)$ is obtained by using a RKHS. In a second step, since the *ab initio* calculations were carried out at Gauss-Legendre points, it is straightforward to expand the 2d-PES $W(R,\alpha)$, in terms of Legendre polynomials $P_\lambda(\cos\alpha)$ as follows,

$$W(R,\alpha) = \sum_{\lambda=0}^{10} f_\lambda(R)P_\lambda(\cos\alpha), \tag{1}$$

where $f_\lambda(R)$ are radial coefficients and λ is their order. Again, an RKHS interpolation is used along the R coordinate. For the global PES for the system, the local PESs determined for the three grids corresponding to the relevant channels of the reaction (Figure 1) are joined. The global PES is thus the weighted sum of the three asymptotic PESs:

$$V(\mathbf{x}) = \sum_{j=1}^{3} w_j(\mathbf{x})V_j(\mathbf{x}) \tag{2}$$

where $\mathbf{x} = (r_{12}, r_{13}, r_{23})$ are the three interatomic distances of the NO_2 molecule (Figure 1), and $V_1(\mathbf{x})$, $V_2(\mathbf{x})$ and $V_3(\mathbf{x})$ are the potential energies for the three regions for which the distances r_{12} (N-O1), r_{13} (N-O2) and r_{23} (O1-O2) are small, and the remaining distances vary from small to large, respectively. The weights $w_j(\mathbf{x})$ are coordinate-dependent and result from the normalization of the following weight functions,

$$w_{j0}(x_j) = \exp(-x_j/\Delta R), \tag{3}$$

$$w_j(x_j) = \frac{w_{j0}(x_j)}{\sum\limits_{l=1}^{3} w_{l0}(x_l)} \tag{4}$$

where $\Delta R = 0.05$ a_0. A similar weighting function was successfully used in Multisurface Adiabatic Reactive Molecular Dynamics (MS-ARMD) which uses the energy as the control parameter in connecting multiple force fields.[9]

3.3 Molecular Dynamics Simulations

Armed with a globally valid PES, the dynamical evolution of the system is followed by propagating Hamilton's equations of motions subject to initial conditions. The equations of motion are integrated numerically using the Velocity-Verlet algorithm.[20] Since the total linear and angular momenta are conserved during the dynamics, it is convenient to select the center of mass of the NO_2 molecule as the origin of the coordinate system. In order to capture the fastest nuclear movements in the system, a time step of 2 a.u. (a.u. means atomic unit of time) (4.84×10^{-2} fs) was used for the propagation. Trajectories were started from an initial separation of (min(15 a_0, impact parameter + 5 a_0)) and followed until the fragments had separated to the same distances. If this criterion was not met, integration continued for a maximum time of the estimated interactionless time of flight through the "reaction-zone" plus

an additional 100 ps, during which most of the NO_2 molecules decayed except for very few low-energy (low E_c and low rovibrational state of initial NO) trajectories.

Suitable initial conditions for NO were generated from a WKB[21]-quantized periodic orbit of the corresponding rotating Morse oscillator for given vibrational v and rotational j quantum numbers.[22] The symmetry axis of the NO molecule and the axis of its rotation, which are orthogonal to each other, was also randomly orientated as was the NO angular momentum. Sampling of the initial rovibrational quantum states of NO, the impact parameter (b) and the collision energy (E_c) is discussed in the next section.

For characterizing the reaction at a given temperature, 4 different cases (I to IV) are considered:

(I) corresponds to NO_2-formation in the high-pressure limit. The NO_2 molecule stabilizes through collisions with the environment. We will indicate this by "∞" as superscript ($k^\infty(T)$). For the formation of NO_2 the same criterion as in Ref. [12] is assumed, that is, the oxygen atom O2 is captured once it approaches to within less than 3.78 a_0 of the center of mass of NO1.

(II) is for NO_2 formation and survival which carries the label "NO_2" as superscript ($k^{NO_2}(T)$). For this case, the "oxygen capture criterion" (see item (I)) is combined with a lifetime criterion, defined as $t_{life} = t_{traj} - t_{tof} > 0$. Here, t_{traj} is the total time of the trajectory, which is either (a) $t_{traj} = 100$ ps for the case that NO_2 does not dissociate or (b) the time until any of the interatomic separations is larger than the initial separation of NO1-O2. The interactionless time of flight $t_{tof} = 2\sqrt{(R_{ini}^2 - b^2)}/v_{ini}$ is determined from the initial conditions.

Case (III) is the oxygen atom exchange reaction, "ex" with associated rate coefficient $k^{ex}(T)$. The criterion for this case is that the N-O2 distance is small and the N-O1 or O1-O2 distances are large.

Process (IV) refers to oxygen molecule formation (O1O2+N) and the corresponding rate coefficient is $k^{O_2+N}(T)$. This case is encountered if the O1-O2 distance is small and the N-O1 or N-O2 distances are large.

3.4 Monte Carlo calculation of the thermal rate coefficients

The thermal rate coefficient[23, 24, 25] can be determined from

$$k(T_e, T_t, T_{rv}) = \frac{\beta_t}{g(T_e)} \sqrt{\frac{8\beta_t}{\pi\mu}} \int_0^\infty \sigma(E_c; T_{rv}) E_c e^{-\beta_t E_c} dE_c, \tag{5}$$

where $\beta_t = k_B T_t$ and k_B is the Boltzmann constant, T_t, T_e, T_{rv} are the translational temperature of NO and O, the electronic temperature of NO and the rovibrational temperature of NO, respectively, $g(T_e)$ is the electronic degeneracy factor,[11, 26] μ is the reduced mass of NO1 and O2, and $\sigma(E_c; T_{rv})$ is the integral cross section as a function of the collision energy, E_c and T_{rv}. In our studies it was assumed that $T_t = T_e = T_{rv}$. In other words, the various degrees of freedom in the reactants are in thermal equilibrium. If no subscript is shown for T then it corresponds to the common temperature. In a similar manner, the reaction cross section $\sigma(E_c; T_{rv})$ for a given collision energy E_c is

$$\sigma(E_c; T_{rv}) = \frac{\sum_{v=0}^{vmax} \sum_{j=0}^{jmax(v)} (2j+1) e^{-\beta_{rv} E_{vj}} \sigma_{vj}(E_c; vj)}{\sum_{v=0}^{vmax} \sum_{j=0}^{jmax(v)} (2j+1) e^{-\beta_{rv} E_{vj}}} \tag{6}$$

where $\sigma_{vj}(E_c)$ is the (v, j)−state dependent cross section at collision energy E_c. The energy E_{vj} of a rovibrational state (v, j) is calculated according to a Morse oscillator model for the NO molecule.[22] The cross section as an integral of the opacity function $P_{vj}(b; E_c)$ for given E_c and rovibrational state (v, j) is

$$\sigma_{vj}(E_c) = \int_0^\infty P_{vj}(b; E_c) 2\pi b \, db \qquad (7)$$

Assuming a thermal distribution of the reactants O(^{3}P) and NO($^2\Pi$) the expression for the electronic degeneracy factor $g(T_e)$ is

$$g(T_e) = [5 + 3\exp(-227.8\,\mathrm{K}/T_e) + \exp(-326.6\,\mathrm{K}/T_e)]\,[1 + \exp(-177.1\,\mathrm{K}/T_e)]. \qquad (8)$$

The integral in Eq. 5 can be calculated by using an Importance Sampling Monte Carlo scheme.[27] For this, the vibrational and rotational quantum numbers v and j, and the collision energy (E_c) are sampled according to Boltzmann distribution.

4 Results and discussion

4.1 The ground state $1^2A'$ PES

The smoothness of the RKHS interpolation is evident in the contour plots of Figure 2. In panel (a), the PES for the "NO1+O2" channel is shown. The global minimum was found at $R_1 = 3.21\ a_0$ and $\alpha_1 = 150.8°$ ($r_{NO} = 2.25\ a_0$ and $\theta_{O-N-O} = 133.1°$ (Table 1) in internal coordinates). The PES for the "O1O2+N" channel is reported in panel (b). Two symmetric minima are observed for the same R_3 Jacobi distance which is measured from the center of mass of O$_2$ to the N atom.

Some features of our ground state PES are summarized in Table 1 and compared to results from previous calculations[13] (using icMRCI+Q/cc-pVQZ with CASSCF(13,10)) and to experiments[28, 29, 30, 31, 32] (high-resolution microwave spectroscopy[29] and laser induced fluorescence[31]). Good agreement with previous computations and experiments was found from the methods used in the present work.

4.2 Thermal rate coefficients

A total of 10 000 individual trajectories was run at each temperature, including $T = 100, 200, 300, 400, 1000, 1500, 2000, 2700, 5000, 7000, 10000, 15000$ and 20000 K. In the following, the thermal rate coefficients obtained from the trajectory calculations are presented.

In Figure 3, the thermal rate coefficients for NO$_2$ formation in the high-pressure limit, $k^\infty(T)$, are shown and compared with published computational and experimental results. Even though the major interest here concerns the high-temperature range, these data provide a validation of the computational procedure put forward in the present work. We report the error bar as twice the standard deviation (σ_S) in order to include 95.4 % of the cases in the confidence interval. In the following it is important to emphasize that the present results are from simulations using the $1^2A'$ PES only (open squares with solid line). The present results are in reasonable agreement with results from previous calculations [11] (solid down-oriented triangles) which also used the $1^2A'$ PES only, although with a different parametrization.
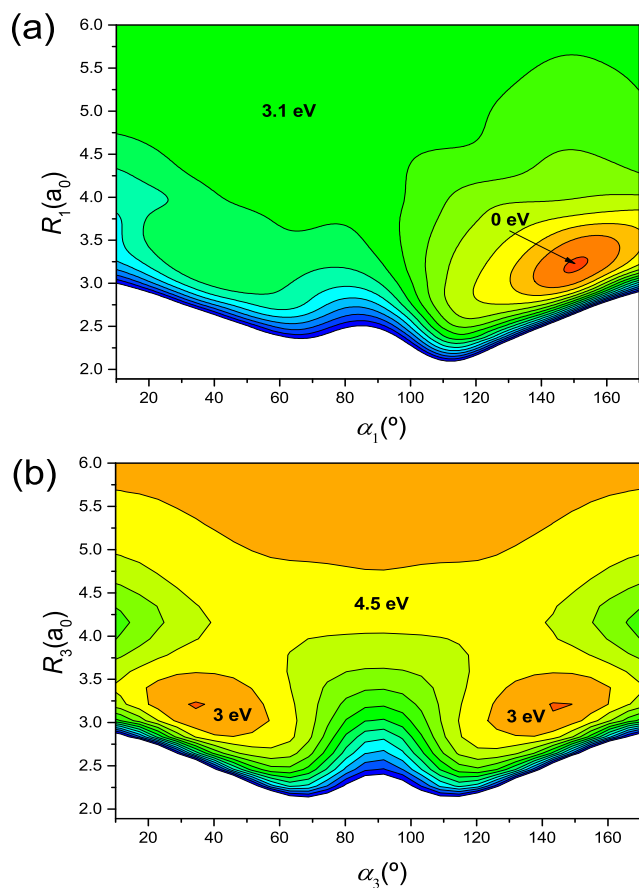
Figure 2: Contour plots for the NO1+O2 (panel a) and O2O1+N (panel b) grids in R_1, α_1 and R_3, α_3 Jacobi coordinates, respectively. The N-O1 (r_1) and O2-O1 (r_3) distances were set to 2.25 a_0. In both cases the contour levels are separated by 0.5 eV.

Both calculations underestimate the experimentally determined thermal rate coefficients at $T = 200$, 300 and 400 K (solid circles and squares). At 2700 K the computed rate coefficient compares favourably with experimental data.[33, 34]

No correction was made for ZPE and other quantum effects, such as tunneling through the centrifugal barrier which can be still significant at low temperatures. The centrifugal barrier originates from the conservation of the total angular momentum and consists of the rotational energy associated with the orbital angular momentum of the colliding partner with respect to the center of mass of the whole system. The orbital angular momentum is directly proportional to the impact parameter and with the initial relative momentum of reactants. An increase of the thermal rate coefficient for lower temperatures has been found to be related to tunneling through the entrance barrier in the reaction of OH with methanol ($T < 200$ K) and O(^{3}P) with alkenes ($T \sim 20$ K).[35, 36] This has also been shown in theoretical studies of HCOH isomerizations.[37] On the other hand, results when using the two lowest $1^2\text{A}'$ and $1^2\text{A}''$ PESs indicate that the $1^2\text{A}''$ PES might play an important role along with quantum

Table 1: Equilibrium geometries and normal mode frequencies from the present work and from reference[13] and experiments. The variables $r_{1,e} = r_{2,e}$, θ_{O-N-O} and D_e are the equilibrium N-O distance, the O-N-O angle and the well depth for the global minimum of NO_2, respectively.

Equilibrium NO_2	Present work	Ref. [13]	Experiments
$r_{1,e} = r_{2,e}$ (a$_0$)	2.25	2.26	2.255 [29]
$\theta_{O-N-O}(^o)$	133.1	134.3	133.9 [29]
D_e(eV)	3.21	3.11	3.23 [30, 31, 32]
Normal frequencies (cm^{-1})			
Symmetric stretch	1322.7	1333.6	1319.794 [28]
Asymmetric stretch	1623.3	1658.0	1616.852 [28]
Bending mode	759.6	755.0	749.649 [28]

effects at temperatures below 400 K. However, for temperatures above 1000 K the results using only the $1^2A'$ PES reasonably match with the experimental results, e.g. for 1500 and 2700 K. This can be explained by noting that the well of the electronically excited C-state of NO_2 (C $1^2A''$) is comparatively small and leads to redissociation of NO_2 at high temperatures [11]. Given this, the influence of tunneling and the $1^2A''$ PES at high temperature appear to be negligible.

For practical work in reaction networks[39] it is advantageous to use a parametrized form for $k^\infty(T)$. A previously considered empirical expression[11] has been fitted to the results from simulations using the $1^2A'$ PES,

$$k^\infty(T)/(10^{-11}\text{cm}^3/\text{s}) = 2.715 + 0.4490 \ln T/\text{K} + 0.3385 \left(\ln T/\text{K}\right)^2 - 0.7134 \left(\ln T/\text{K}\right)^3. \quad (9)$$

This yields the red solid line in Figure 3.

The thermal rate coefficients for temperatures between $T = 5000$ K and $T = 20000$ K are reported in Figure 4 for cases I to IV studied in this work. With increasing temperature a slight increase in the thermal rate coefficients is found. At 20000 K, they increase to $k^\infty = 5.5 \cdot 10^{-11}$ cm^3/s, $k^{\text{NO}_2} = 3.4 \cdot 10^{-11}$ cm^3/s, $k^{\text{ex}} = 1.9 \cdot 10^{-11}$ cm^3/s and $k^{\text{O}_2+\text{N}} = 0.65 \cdot 10^{-11}$ cm^3/s. As could be expected, results with and without ZPE correction agree to within the error bars. Again, for practical purposes the data for $k^\infty(T)$ were fitted to a linear equation as (solid line in Figure 4)

$$k^\infty(T) \ /(10^{-11}\text{cm}^3/\text{s}) = 2.497 + 0.1529(T/\text{K}). \quad (10)$$

For a more detailed description of the O_2 production channel, Figure 5 (panel (a)) reports the fraction of initial vibrational energy of NO relative to the total energy *versus* the vibrational quantum number of NO (v_{NO}) for 8 values of the collision energy. The fraction of collision energy is complementary to the vibrational energy to give the total energy of the system ($E_\text{c} + E_\text{vib} = E_\text{tot}$). In panel (b), the contour plot of the channel probability is shown. In all cases, the rotational ground state ($j_{\text{NO}} = 0$) is assumed. For this calculation, 2500 trajectories were run for each combination of $E_\text{c} =$ {0.82, 1.09, 1.36, 2.18, 2.72, 4.08, 4.63, 5.44} eV and $v_{\text{NO}} =$ {0, 1, 2, 3, 4, 6, 9, 12, 15, 20} values. The results indicate that for $v_{\text{NO}} = 0$ the O_2-channel opens only for very high collision energies (> 4.63 eV). However, for an initial NO-state with $v_{\text{NO}} = 9$ (corresponding to $E_\text{c} = 0.82$ eV) production of 0.6 %
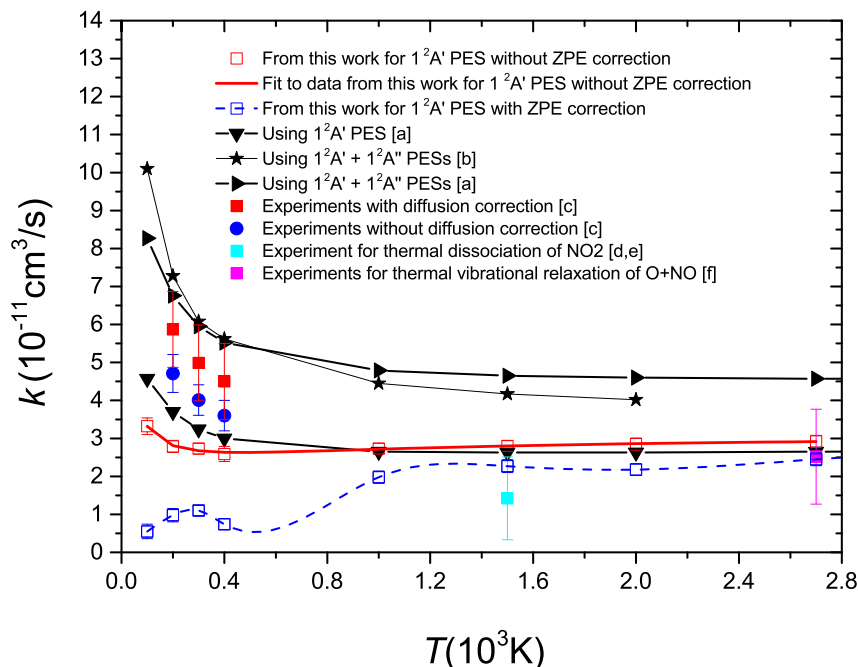
Figure 3: Thermal rate coefficients for the NO_2 formation in the high-pressure limit, $k^{\infty}(T)$ *versus* temperature. In the legend, [a]=Ref.[11], [b]=Ref.[12], [c]=Ref.[10], [d]=Ref.[33], [e]=Ref.[34], and [f]=Ref.[38]

of O_2 is observed. This qualitatively follows from Polanyi's rule [23] which predicts that the reaction should go to the late-barrier "O_2 + N" channel when the NO molecule is initially vibrationally highly excited even for low collision energies. In order to give a clearer picture of this, let us assume we start the reaction coming from $N+O_2$ (left side in Figure 1). In this situation, the reactants experience an early barrier of about 1.3 eV (Figure 1 and 3 b). The exit channel in this case is barrierless (NO1 + O2). According to Polanyi's rule, the excess energy released after crossing the early barrier goes predominantly into the internal degrees of freedom in the products (NO1) rather than into their (relative) translational energy.

For the set of vibrational quantum numbers and energies studied, the maximum channel probability of 13 % for O_2−formation is reached at $v_{NO} = 20$. In general, the trend indicates that for lower vibrational quantum numbers, more energy needs to be in the translational degree of freedom. Conversely, for higher vibrational excitation of the NO, less collision energy is required. When both the collision energy and the vibrational quantum number of NO are high, the reaction probability of $N+O_2$ formation is maximal.

5   Conclusions

The $O(^3P) + NO(^2\Pi)$ reaction has been studied over a range of temperatures relevant for the hypersonic flight regime (5000-20000 K). For this purpose the thermal cross sections and rate coefficients were calculated for the different exit channels. The results indicate that oxygen
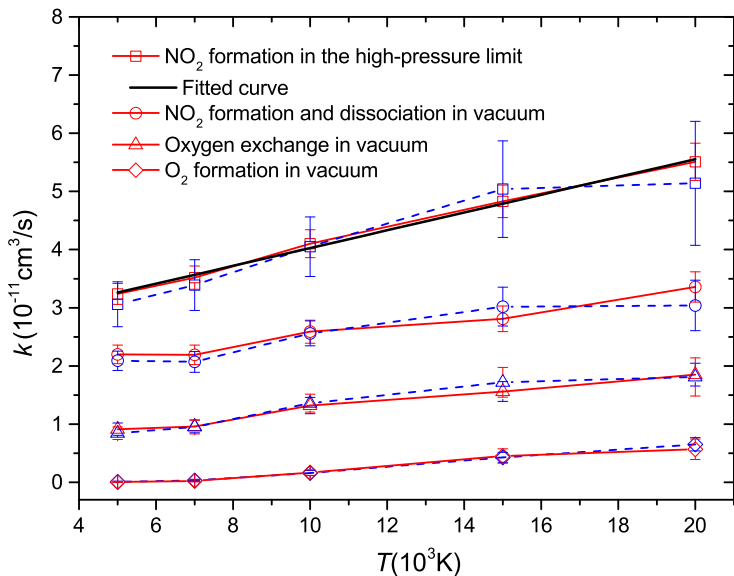
Figure 4: High-pressure limit thermal rate coefficients for NO_2 formation (squares) (fit with black solid line), NO_2 formation and dissociation (circles), oxygen exchange channel (up-oriented triangles) and oxygen production channel (diamonds).

exchange (NO2+O1) occurs at all temperatures. However O_2-formation is only found for $T \geq$ 5000 K. For both channels, the thermal rate coefficient increases as the temperature increases ($T = 5000$ to 20000 K). A more detailed scrutiny of the "O1O2+N" channel indicates that the smaller the vibrational quantum number of NO, the higher translational energy is required to open it; and the contrary, the higher the vibrational quantum number, the less translational energy is needed. Our results for lower temperatures are discussed and compared to previous experimental and computational results. In this respect, this work also presents the validation of an efficient computational protocol for the investigation of reaction dynamics of triatomic systems. Two aspects make the approach efficient and accurate. Firstly, the *ab initio* energies are handled by means of a RKHS representation which is accurate, computationally convenient and correctly describes the asymptotic regions of the PESs. Secondly, thermal quantities are calculated by using Importance Sampling which is efficient to evaluate multi-dimensional integrals over the phase-space of initial states. With less than 1000 classical trajectories a relative error below 10 % for the rate coefficients is obtained.

6   Outlook

The present work is the basis for computing state-selected cross sections and rate constants for the reaction considered. More broadly, the computational framework discussed here can be generalized to other relevant reactions for the hypersonic flight regime. Working along the lines put forward in the present report, starting from electronic structure calculations, building the fully-dimensional, reactive PES is almost automatic as is generation of the initial
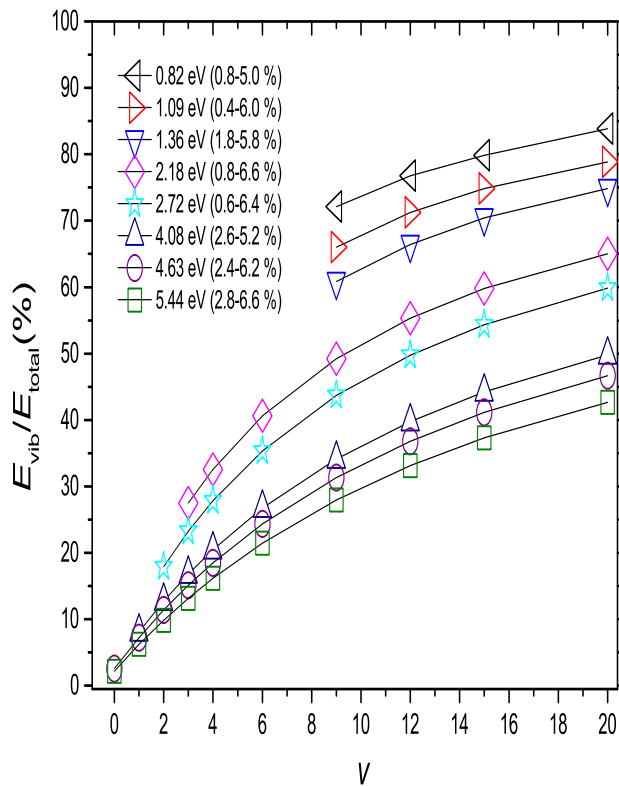
Figure 5: Fraction of initial vibrational energy of NO with respect to the total energy *versus* the vibrational quantum number for 8 values of the collision energy (panel (a)). The contour plot of the channel probability as percentage is shown in panel (b). Only data for "O_2+N" channel are shown.

conditions and running the necessary atomistic simulations. This provides the raw data for the computation of the rate coefficients at temperatures for which concrete experiments is difficult and which is the major information sought for incorporation into the chemical modeling. Pursuing this for additional relevant reactions and including the effect of electronically excited states will be of particular interest for the continuation of this project.

Acknowledgments

References

[1] K Yoshino, JR Esmond and WH Parkinson, Chem. Phys. **221(1,2)**, 169–174 (1997).

[2] W Schneider, GK Moortgat, GS Tyndall and JP Burrows, J. Photochem. Photobiol. A **40(2,3)**, 195–217 (1987).

[3] TC Corcoran, EJ Beiting and MO Mitchell, J. Molec. Spectrosc. **154(1)**, 119–128 (1992).

[4] TE Schwartzentruber, LC Scalabrin and ID Boyd, J. Spacecraft Rockets **45(6)**, 1196–1206 (2008).

[5] S. Mishra and M. Meuwly. *Kinetics and Dynamics: from Nano- to Bio-Scale, Challenges and Advances in Computational Chemistry and Physics.* Series: Challenges and Advances in Computational Chemistry and Physics, Vol. 12. Springer, Berlin, (2010).

[6] R. B. Gerber, V. Buch and Mark A. Ratner, J. Chem. Phys. **77(6)**, 3022–3030 (1982).

[7] M.H. Beck, A. Jckle, G.A. Worth and H. D. Meyer, Phys. Rep. **324(1)**, 1–105 (2000).

[8] H. Wang and M. Thoss, J. Chem. Phys. **119(3)**, 1289–1299 (2003).

[9] T Nagy, J Yosa and M Meuwly, J. Chem. Theory. Comput. **10(4)**, 1366–1375 (2014).

[10] H Hippler, M Siefke, H Stark and J Troe, Phys Chem Chem Phys. **1(1)**, 57–61 (1999).

[11] LB Harding, H Stark, J Troe and VG Ushakov, Phys Chem Chem Phys. **1(1)**, 63–72 (1999).

[12] MV Ivanov, H Zhu and R Schinke, J. Chem. Phys. **126( )**, 054304 (2007).

[13] V Kurkal, P Fleurat-Lessard and R Schinke, J. Chem. Phys. **119(3)**, 1489–1501 (2003).

[14] Thom H. Dunning, J. Chem. Phys. **90(2)**, 1007–1023 (1989).

[15] Rick A. Kendall, Thom H. Dunning and Robert J. Harrison, J. Chem. Phys. **96(9)**, 6796–6806 (1992).

[16] Stephen R. Langhoff and Ernest R. Davidson, Int. J. Quantum Chem. **8(1)**, 61–72 (1974).

[17] Wl/odzisl/aw Duch and Geerd H. F. Diercksen, J. Chem. Phys. **101(4)**, 3018–3030 (1994).

[18] H. J. Werner, P. J. Knowles, G. Knizia, F. R. Manby and M. Schütz, WIREs Comput Mol Sci **2**, 242–253 (2012).

[19] T. S. Ho and H. Rabitz, J. Chem. Phys. **104(7)**, 2584–2597 (1996).

[20] Loup Verlet, Phys. Rev. **159**, 98–103Jul 1967.

[21] R. L. Liboff. *Introductory Quantum Mechanics (4th ed.).* Addison-Wesley, Massachusetts, (2003).

[22] R. N. Porter, L. M. Raff and W. H. Miller, J. Chem. Phys. **63(5)**, 2214–2218 (1975).

[23] R. D. Levine. *Molecular Reaction Dynamics.* Cambridge University Press, Cambridge, (2005).

[24] M. Brouard. *Reaction Dynamics.* Oxford Chemistry Primers 61 (Oxford Science Publications), Oxford, (1998).

[25] F. Y. Hansen N. E. Henriksen. *Theories of molecular reaction dynamics. The microscopic foundation of chemical kinetics.* Oxford Graduate Texts, Oxford, (2012).

[26] James W. Duff and Ramesh D. Sharma, J. Chem. Soc., Faraday Trans. **93**, 2645–2649 (1997).

[27] D. Frenkel and B. Smit. *Understanding Molecular Simulation. From Algorithms to Applications (2nd Edition).* Academic Press, London, (2001).

[28] A. Delon and R. Jost, J. Chem. Phys. **95(8)**, 5686–5700 (1991).

[29] WC Bowman and FC De Lucia, J. Chem. Phys. **77(1)**, 92–107 (1982).

[30] R Jost, J Nygrd, A Pasinski and A Delon, J. Chem. Phys. **105(3)**, 1287–1290 (1996).

[31] Robert Georges, Antoine Delon and Rmy Jost, J. Chem. Phys. **103(5)**, 1732–1747 (1995).

[32] K. P. Huber and G. Herzberg. *Molecular Spectra and Molecular Structure and IV. Constants of Diatomic Molecules.* Van Nostrand, Princeton, (1979).

[33] J. Troe, Berichte der Bunsengesellschaft für physikalische Chemie **73(2)**, 144–147 (1969).

[34] Michael Rhrig, Eric L. Petersen, David F. Davidson and Ronald K. Hanson, Int. J. Chem. Kinet. **29(7)**, 483–493 (1997).

[35] Hassan Sabbah, Ludovic Biennier, Ian R. Sims, Yuri Georgievskii, Stephen J. Klippenstein and Ian W. M. Smith, Science **317(5834)**, 102–105 (2007).

[36] I. R. Sims, Nat. Chem. **5**, 734–736 (2013).

[37] Jingjing Zheng, Xuefei Xu, Ruben Meana-Paneda and Donald G. Truhlar, Chem. Sci. **5**, 2091–2099 (2014).

[38] K. Glanzer and J. Troe, J. Chem. Phys. **63(10)**, 4352–4357 (1975).

[39] V. Wakelam, I.W.M. Smith, E. Herbst, J. Troe, W. Geppert, H. Linnartz, K. Öberg, E. Roueff, M. Agndez, P. Pernot, H.M. Cuppen, J.C. Loison and D. Talbi, Space Science Reviews **156(1-4)**, 13–72 (2010).